Int J Comput Vis
DOI 10.1007/s11263-012-0586-8

Teichmüller Shape Descriptor and Its Application to Alzheimer's Disease Study

Wei Zeng · Rui Shi · Yalin Wang · Shing-Tung Yau · Xianfeng Gu · Alzheimer's Disease Neuroimaging Initiative

Received: 14 December 2011 / Accepted: 4 October 2012

Abstract We propose a novel method to apply Teichmüller space theory to study the signature of a family of nonintersecting closed 3D curves on a general genus zero closed surface. Our algorithm provides an efficient method to encode both global surface and local contour shape information. The signature—Teichmüller shape descriptor—is computed by surface Ricci flow method, which is equivalent to solving an elliptic partial differential equation on surfaces and is numerically stable. We propose to apply the new signature to analyze abnormalities in brain cortical morphometry. Experimental results with 3D MRI data from Alzheimer's disease neuroimaging initiative dataset [152 healthy control subjects versus 169 Alzheimer's disease (AD) patients] demonstrate the effectiveness of our method and illustrate its potential as a novel surface-based cortical morphometry measurement in AD research.

Keywords Teichmüller space · Conformal welding · Shape analysis

W. Zeng (✉)
Florida International University, Miami, FL, USA
e-mail: wzeng@cs.fiu.edu

R. Shi · X. Gu
State University of New York at Stony Brook, Stony Brook, NY, USA
e-mail: rshi@cs.sunysb.edu
e-mail: gu@cs.sunysb.edu

Y. Wang
Arizona State University, Tempe, AZ, USA
e-mail: ylwang@asu.edu

S.-T. Yau
Harvard University, Cambridge, MA, USA
e-mail: yau@math.harvard.edu

1 Introduction

Some neurodegenerative diseases, such as Alzheimer's disease (AD), are characterized by progressive cognitive dysfunction. The underlying disease pathology most probably precedes the onset of cognitive symptoms by many years. Efforts are underway to find early diagnostic biomarkers to evaluate neurodegenerative risk presymptomatically in a sufficiently rapid and rigorous way. Among a number of different brain imaging, biological fluid, and other biomarker measurements for use in the early detection and tracking of AD, structural magnetic resonance imaging (MRI) measurements of brain shrinkage are among the best established biomarkers of AD progression and pathology.

In structural MRI studies, early researches (Thompson and Toga 1996; Fischl et al. 1999) have demonstrated that surface-based brain mapping may offer advantages over volume-based brain mapping work (Ashburner et al. 1998) to study structural features of the brain, such as cortical gray matter thickness, complexity, and patterns of brain change over time due to disease or developmental processes. In research studies that analyze brain morphology, many surface-based shape analysis methods have been proposed, such as spherical harmonic analysis (Gerig et al. 2001; Chung et al. 2008), minimum description length approaches Davies et al. 2003, medial representations (M-reps) (Pizer et al. 1999), cortical gyrification index (Tosun et al. 2006), shape space (Liu et al. 2010), metamorphosis (Trouve and Younes 2005), momentum maps (Qiu and Miller 2008), conformal invariants (Wang et al. 2009), and so on; these methods may be applied to analyze shape changes or abnormalities in cortical and subcortical brain structures. Among these approaches, most of them relied on local geometric features, e.g., thickness or distance. In contrast, our method focuses on both local geometries of functional regions and

Journal: **11263** MS: **0586** ☐ TYPESET ☐ DISK ☐ LE ☐ CP Disp.:**2012/10/24** Pages: **16** Layout: **Large**

geometric relations among them. When the regions with the same local geometries are glued together with a different pattern, introducing some twisting or tensions, our signatures will be changed significantly. Our Teichmüller shape space approach provides measurements on the intrinsic conformal structure by computing global intrinsic angle-invariant shape descriptors. This local–global view based on conformal geometry would be highly advantageous for AD biomarker research.

In order to compute the conformal welding signature, we need to map each functional area onto the planar domain first. This can be accomplished by using the Ricci flow method. Ricci flow is a powerful tool to compute the conformal structures for any arbitrary surfaces. It has been successfully used to prove the Poincaré conjecture. Ricci flow deforms a Riemannian metric conformally according to curvature proportionally like a heat diffusion process such that the curvatures evolve and eventually become constant everywhere. The discrete surface Ricci flow has been presented in (Jin et al. 2008; Zeng et al. 2010; Wang et al. 2012).

1.1 AD-Related Motivation

MRI-based measures of atrophy are regarded as valid markers of AD state and progression. Atrophy of brain structures is associated with cognitive impairment in normal aging and AD (Frisoni et al. 2010; Fox et al. 1999), and typically results from a combination of neuronal atrophy, cell loss, and impairments in myelin turnover and maintenance, and corresponding reductions in white matter volume. These cellular processes combine at the macroscopic level to induce observable differences on brain MRI. Several of processes (such as cellular atrophy) occur with normal aging, and others (including neuronal loss) are further promoted by amyloid plaque and neurofibrillary tangle deposition. Although surface expansion and contraction are less traditional measures of morphometry, it is likely that they simply reflect the same processes that cause progressive brain tissue loss.

Our work, as well as some approaches developed by other groups [e.g., Jack et al. (2004); Cuingnet et al. (2011); Chincarini et al. (2011); Wang et al. (2011)], measures the extent and severity of cortex volume, grey matter thickness, hippocampal and ventricular shape deformations as a proxy for grey matter loss, hippocampal atrophy and ventricular enlargement. The detected compression (or expansion for lateral ventricle) of the surface areas is associated with macrostructural and microstructural loss in different brain regions and makes them useful indices of the neurodegenerative process. Besides grey matter thickness, it would be beneficial to have a stable surface area related statistics. The Teichmüller shape signature we proposed here is such a feature set which quotients out scaling, translation, rotation, general isometric deformation, and conformal deformation and enables a more exact comparison of brain cortex changes. In addition, our signature depicts the correlations between AD-related functional areas (see Shi et al. 2011) and the whole brain cortical surface, and has the powerful ability to recover the shape of the whole brain surface. All of these motivate us to apply the new signature to AD detection and we believe it will pave a novel way for shape analysis in AD study.

This work was inspired by Sharon and Mumford's work Sharon and Mumford (2006) and generalized the idea from 2D shape space to 3D shape space. We propose a novel and intrinsic method to compute the global correlations between various surface region contours in Teichmüller space and apply it to study brain morphology in AD. The proposed shape signature demonstrates the global geometric features encoded in the regions of interest (ROI), which are regarded as a biomarker for measurements of AD progression and pathology. It is based on the brain surface conformal structure (Hurdal and Stephenson 2004; Angenent et al. 2000; Gu et al. 2004; Wang et al. 2007) and can be accurately computed using the discrete surface Ricci flow method (Jin et al. 2008; Zeng et al. 2010; Wang et al. 2006). Theoretically, the signature is guaranteed to be a complete and global shape descriptor based on Teichmüller space theory and conformal welding theory.

1.2 Related Work

In this work, we perform AD detection by studying the morphometry of brain cortical surface. Besides the discussion of AD detection applications in the above, here, we first review the literature on brain morphometry study research. Due to our method is based on conformal brain mapping, we then review surface-based brain mapping methods, which are closely related to surface parameterizations. Furthermore, we review the work of Sharon and Mumford Sharon and Mumford (2006), which inspired our current conformal welding signature.

In *brain morphometry study research*, volumetric measures of structures identified on 3D MRI have been used to study group differences in brain structure and also to predict diagnosis (Ashburner et al. 1998). Recent work has also used shape-based features (Liu et al. 2010; Trouve and Younes 2005; Qiu and Miller 2008) and conformal invariants (Wang et al. 2009) analyzing surface changes using pointwise displacements of surface meshes, local deformation tensors, or surface expansion factors, such as the Jacobian determinant of a surface based mapping. For closed surfaces homotopic to a sphere, spherical harmonics have commonly been used for shape analysis, as have their generalizations, e.g., eigenfunctions of the Laplace–Beltrami operator in a system of spherical coordinates. These shape indices are also rotation invariant, i.e., their values do not depend on the orientation

Journal: 11263 MS: 0586 TYPESET DISK LE CP Disp.:2012/10/24 Pages: 16 Layout: Large

of the surface in the embedding space (Thompson and Toga 1996; Gerig et al. 2001; Shen et al. 2007). Chung et al. (2008) proposed a weighted spherical harmonic representation. For a specific choice of weights, the weighted SPHARM is shown to be the least square approximation to the solution of an anisotropic heat diffusion on the unit sphere. Davies et al. Davies et al. (2003) performed a study of anatomical shape abnormalities in schizophrenia, using the minimal distance length approach to statistically align hippocampal parameterizations. For classification, linear discriminant analysis or principal geodesic analysis can be used to find the discriminant vector in the feature space for distinguishing diseased subjects from healthy control subjects. Tosun et al. (2006) proposed the use of three different shape measures to quantify cortical gyrification and complexity. Gorczowski (2007) presented a framework for discriminant analysis of populations of 3D multi-object sets. In addition to a sampled medial mesh representation (Pizer et al. 1999), they also considered pose differences as an additional statistical feature to improve the shape classification results. Based on discrete Laplace-Beltrami operator, heat kernel method (Chung et al. 2005) was also applied to 3D biological shape analysis (Lai et al. 2010).

For *brain surface parameterization research*, Schwartz et al. (1989) and Timsari and Leahy (2000) computed quasi-isometric flat maps of the cerebral cortex. Hurdal and Stephenson (2004 reported a discrete mapping approach that uses circle packings to produce "flattened" images of cortical surfaces on the sphere, the Euclidean plane, and the hyperbolic plane. Angenent et al. (2000) implemented a finite element approximation for parameterizing brain surfaces via conformal mappings. Gu et al. (Gu et al. 2004) proposed a method to find a unique conformal mapping between any two genus zero manifolds by minimizing the harmonic energy of the map. The holomorphic 1-form based conformal parameterization (Wang et al. 2007) can conformally parameterize high genus surfaces with boundaries but the resulting mappings have singularities. Other brain surface conformal parametrization methods, the Ricci flow method (Wang et al. 2006) and slit map method (2008), can handle surfaces with complicated topologies (boundaries and landmarks) without singularities. Wang et al. (2009) applied the Yamabe flow method to study statistical group differences in a group of 40 healthy controls and 40 subjects with Williams syndrome, showing the potential of these surface-based descriptors for localizing cortical shape abnormalities in genetic disorders of brain development.

Conformal mappings have been applied in computer vision for modeling the 2D shape space by Sharon and Mumford (2006). The image plane is separated by a 2D contour, both interior and exterior are conformally mapped to disks, then the contour induces a *diffeomorphism* of the unit circle (a differentiable and invertible, periodic function), which is the signature of the contour. The signature is invariant under translations and scalings, and able to recover the original contour by *conformal welding*. Later, this method is generalized to model multiple 2D contours with inner holes in Lui et al. (2010). To the best of our knowledge, our method is the first one to generalize Sharon and Mumford's 2D shape space to 3D surfaces, also from simply connected domains to multiply connected domains. The proposed signature considers the correlation of the regions surrounded by separate closed contours.

1.3 Our Approach

For a 3D surface, all the contours (simple closed curves on the 3D surface) represent the "shape" of the surface. Inspired by the beautiful research work of Sharon and Mumford (2006) on 2D shape analysis [recently it has been generalized to model multiple 2D contours Lui et al. (2010)], we build a Teichmüller space for 3D shapes using conformal mappings. In this Teichmüller space, each 3D shape is represented by a point in the space; each point denotes a unique equivalence class up to Möbius transformations, which are conformally equivalent transformations.

Given a genus zero closed 3D surface with nonintersecting contours on the surface, each contour surrounds a 3D patch with disk topology; all the contours partition the whole surface to a set of 3D simply-connected patches and a 3D base surface with multiple boundaries. By conformal mapping, the base surface can be mapped to a circle domain where one boundary is mapped to the exterior unit disk, other boundaries are mapped to the interior circles. The centers and radii of all the interior circles form a conformal invariant, called *conformal module*, unique up to Möbius transformations. Similarly, by conformal mapping, each 3D patch is mapped to a unit disk; therefore, each contour has two circle mapping results, one is on the foreground unit disk mapping, the other is on the base circle domain. Then a diffeomorphism of the unit circle is constructed between these two circle mappings to form a shape descriptor for the corresponding contour. For a 3D surface, the conformal module and the diffeomorphisms of all the contours together form a global and unique shape representation of the surface, called *Teichmüller coordinates* in Teichmüller space; and vice versa, the representation can recover the 3D contours on the 3D surface uniquely. By using this signature, the similarities of 3D shapes can be quantitatively analyzed, therefore, the classification and recognition of 3D objects can be performed from their observed contours.

1.3.1 Geometric Intuition

The brain cortical surface is partitioned to different functional regions, each region is conformally mapped to a canonical space such that its boundary curves are mapped to circles.

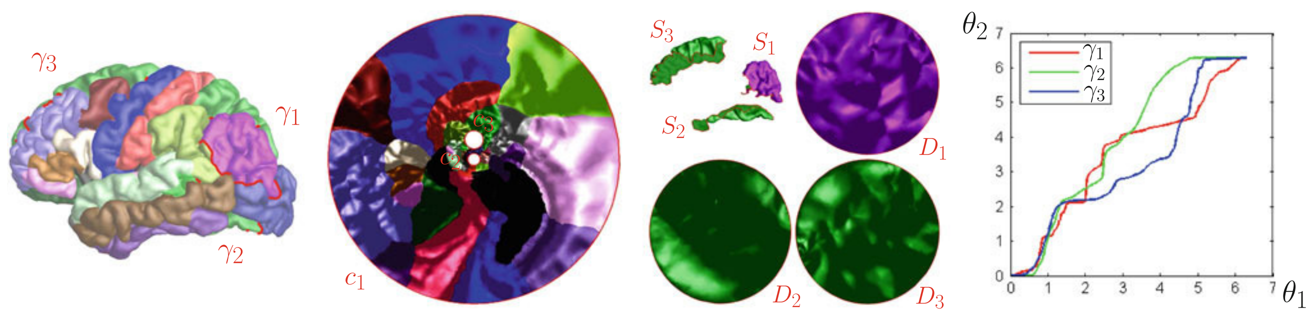

(a) contours on hemisphere brain surface

(b) conformal map of base domain D_0

(c) conformal maps D_1, D_2, D_3

(d) diffeomorphism signature

Fig. 1 Diffeomorphism signature via uniformization mapping for a genus zero surface with 3 simple closed contours. The curve on surface γ_i in (**a**) surrounds the patch S_i in (**c**) and is mapped to the boundary c_i of the circle domain D_i in (**c**). The curve γ_i is also mapped to the boundary of the base circle domain D_0 in (**b**). The curves in (**d**) demonstrate the diffeomorphisms for the 3 contours

Then the boundary of each region induces a diffeomorphism from the unit circle to itself. The shapes of canonical spaces and the automorphisms of the unit circle form the signature.

Intuitively, the signature depends on many factors, not only the geometry of the whole cortical surface and the geometries of the regions, but also (more importantly) the pattern to glue the regions to form the whole surface. For example, if the geometry of one functional area is changed, then part of the signature related to that area will be changed; on the other hand, if we partition the whole surface differently, by enlarging some areas and shrinking the others, or alter the boundary of one area, then the signature will be changed. Furthermore, if some shifting, twisting, or torsion along the gluing boundaries is introduced during the gluing process, then the signature will be changed accordingly. Therefore, the proposed signature has a unique local-global view. Namely, our signatures reflect both the local geometries of regions and the global intrinsic relations among them. Most existing methods emphasize on the geometries of regions, in contrast, our method also emphasizes the geometric relations.

Theoretically, according to Teichmüller theory and conformal welding theory, the boundaries of the regions can be reconstructed from their signatures. Furthermore, the signature is invariant to scaling, translation, rotation, general isometric deformation, and conformal deformation. All the signatures form an abstract Riemannian manifold; the distance among different signatures can be measured by special metrics. The signature is sensitive to the area change and the change of geometric relations. In AD morphometry study, when human brain cortical surface has atrophy, the signature changes correspondingly. For example, if a functional area shrinks, the corresponding circle of the contour decreases to some extent on the canonical domain, the twisting or surface tension change will be reflected by the signature as well.

Our work is based on conformal geometry, which is the study of a set of angle-preserving transformations. All metric oriented surfaces have conformal structures so it is a universal structure for surface study. The Teichmüller space is a quotient space of conformal equivalence relation. Similar to that isometry indicates the deformation that does not change distance between any two points on the surface, a conformal structure induces the deformation that does not change angle structure between any two curves on the surface. So the proposed statistics measures the difference between surfaces with different conformal structures. Among all the diffeomorphisms between the surfaces, there exists a unique one that induces the minimal angle distortion. This distortion can be utilized as the distance.

1.3.2 Contributions

To the best of our knowledge, it is the first work to apply conformal module and contour diffeomorphisms together to brain morphometry research. Our experimental results demonstrate that this novel and simple method may be useful to analyze certain functional areas, and it may shed some lights on detecting abnormality regions in brain surface morphometry. Our major contributions in this work are as follows:

1. A new method to compute Teichmüller shape descriptor, in a way that generalized a prior 2D domain conformal mapping work Sharon and Mumford (2006).
2. The method is theoretically rigorous and general, which presents a stable way to calculate the diffeomorphisms of contours in general 3D surfaces based on surface Ricci flow method.
3. It involves solving elliptic partial differential equations (PDEs), so it is numerically efficient and computationally stable.
4. The shape descriptors are unique, global and invariant to rigid motion and conformal deformations.

Journal: **11263** MS: **0586** ☐ TYPESET ☐ DISK ☐ LE ☐ CP Disp.:**2012/10/24** Pages: **16** Layout: **Large**

1.3.3 Pipeline

Figure 1 shows the pipeline for computing the conformal module and diffeomorphism signature for a 3D surface with 3 closed contours. Here, we use a human brain hemisphere surface whose functional areas are divided and labeled in different color. The contours (simple closed curves) of functional areas can be used to slice the surface open to connected patches. As shown in frames (a–c), three contours $\gamma_1, \gamma_2, \gamma_3$ are used to divide the whole brain (a genus zero surface S) to 4 patches S_0, S_1, S_2, S_3; each of them is conformally mapped to a circle domain (e.g., disk or annuli), D_0, D_1, D_2, D_3. Note that $\gamma_1, \gamma_2, \gamma_3$ are the contours of the inferior parietal area, the fusiform area, and the superior frontal area, respectively. In (b), the base circle domain is normalized by Möbius transformation, such that the circle c_2 is centered at origin, c_3 is centered along imaginary-axis, then conformal module of the base domain is defined as the centers and radii of circles c_2, c_3, i.e., $Mod = (r_2, y_3, r_3) = (0.042263, 0.136767, 0.063546)$, where r_i and $(x_i + iy_i)$ denote the radius and the center of circle c_i, respectively. In the mapping results, one contour is mapped to two circles in two mappings. The representation of the shape corresponding to each contour is a diffeomorphism of the unit circle to itself, defined as a mapping between periodic polar angles $(\theta_1, \theta_2), \theta_1, \theta_2 \in [0, 2\pi]$. The proper normalization is employed to remove Möbius ambiguity. As shown in (d), the curves demonstrate the diffeomorphisms for three contours. The diffeomorphisms induced by the conformal maps of each curve together with the conformal module form a unique shape signature, which is the Teichmüller coordinates in Teichmüller space and may be used for shape comparison and classification.

We tested our algorithm in the segmented regions on a set of brain *left* cortical surfaces extracted from 3D anatomical brain MRI scans from Alzheimer's Disease Neuroimaging Initiative (ADNI) dataset (152 healthy control subjects versus 169 AD patients). The proposed method can reliably compute the shape signatures on three cortical functional areas by computing the conformal modules and the diffeomorphisms of all the three contours. Using these signatures as statistics, our method achieved the 95 percent confidence interval 91.38±0.55 % for the average accuracy rate to differentiate a set of AD patients from healthy control subjects.

1.3.4 Organization

The paper is organized as follows: Sect. 2 introduces the theoretical background on surface uniformization and Teichmüller space and gives the main theorem about the novel shape signature. Section 3 introduces the computation details of the proposed Teichmüller shape descriptor. Numerical experiments and applications to AD study are discussed in Sect. 4. Section 5 concludes the paper and gives the future work. The theoretic proof for the main theorem is detailed in Appendix section.

2 Theoretical Background

In this section, we briefly introduce the theoretical foundations necessary for the current work. For more details, we refer readers to the classical books, such as Riemann surface theory (Farkas and Kra 1991), Teichmüller theory (Gardiner and Lakic 2000), differential geometry (Schoen and Yau 1994), and complex analysis (Henrici 1988).

2.1 Surface Uniformization Mapping

Conformal mapping between two surfaces preserves angles. Suppose $(S_1, \mathbf{g}_1)$ and $(S_2, \mathbf{g}_2)$ are two surfaces embedded in $\mathbb{R}^3$, $\mathbf{g}_1$ and $\mathbf{g}_2$ are the induced Riemannian metrics.

Definition 1 *(Conformal Mapping)* A mapping $\phi : S_1 \to S_2$ is called *conformal*, if the pull back metric of $\mathbf{g}_2$ induced by ϕ on S_1 differs from $\mathbf{g}_1$ by a positive scalar function:

$$\phi^* \mathbf{g}_2 = e^{2\lambda} \mathbf{g}_1, \qquad (1)$$

where $\lambda : S_1 \to \mathbb{R}$ is a scalar function, called the *conformal factor*.

For example, all the conformal automorphisms of the unit disk form the *Möbius transformation group* of the disk, each mapping is given by

$$z \to e^{i\theta} \frac{z - z_0}{1 - \bar{z}_0 z}. \qquad (2)$$

All the conformal automorphism group of the extended complex plane $\mathbb{C} \cup \{\infty\}$ is also called Möbius transformation group, each mapping is given by

$$z \to \frac{az + b}{cz + d}, ad - bc = 1, a, b, d, c \in \mathbb{C}. \qquad (3)$$

By stereo-graphic projection, the unit sphere can be conformally mapped to the extended complex plane. Therefore, the Möbius transformation group is also the conformal automorphism group of the unit sphere.

A circle domain on the complex plane is the unit disk with circular holes. A circle domain can be conformally transformed to another circle domain by Möbius transformations. All genus zero surfaces with boundaries can be conformally mapped to circle domains:

Theorem 1 (Uniformization) *Suppose S is a genus zero Riemannian surface with boundaries, then S can be conformally mapped onto a circle domain. All such conformal mappings differ by a Möbius transformation on the unit disk.*

Journal: 11263 MS: 0586 TYPESET DISK LE CP Disp.:2012/10/24 Pages: 16 Layout: Large

This theorem can be proved using Ricci flow straightforwardly. Therefore, the conformal automorphism group of $SConf(S)$ is given by

$$Conf(S) := \{\phi^{-1} \circ \tau \circ \phi | \tau \in M\ddot{o}b(\mathbb{S}^2)\}. \tag{4}$$

2.2 Teichmüller Space

Definition 2 *(ConformalEquivalence)* Suppose $(S_1, \mathbf{g}_1)$ and $(S_2, \mathbf{g}_2)$ are two Riemann surfaces. We say S_1 and S_2 are *conformal equivalent* if there is a conformal diffeomorphism between them.

All Riemann surfaces can be classified by the conformal equivalence relation. Each conformal equivalence class shares the same *conformal invariants*, the so-called *conformal module*. The conformal module is one of the key component for us to define the unique shape signature.

Definition 3 *(Teichmüller Space)* Fixing the topology of the surfaces, all the conformal equivalence classes form a manifold, which is called the *Teichmüller space*.

The Teichmüller space is a quotient space of conformal equivalence relation. For example, all topological disks (genus zero Riemann surfaces with single boundary) can be conformally mapped to the planar disk. Therefore, the Teichmüller space for topological disks consists of a single point.

All the surfaces in real life are Riemann surfaces, therefore with conformal structures. Two surfaces share the same conformal structure, if there exists a conformal mapping between them. Conformal modules are the complete invariants of conformal structures and intrinsic to surface itself. They can serve as the coordinates in Teichmüller space.

Suppose a genus zero Riemann surface S has b boundary components $\{\gamma_1, \gamma_2, \ldots, \gamma_b\}$, $\partial S = \gamma_1 + \gamma_2 + \ldots + \gamma_b$, $\phi : S \to \mathbb{D}$ is the conformal mapping that maps S to a circle domain $\mathbb{D}$, such that it satisfies the following Möbius normalization conditions,

1. $\phi(\gamma_1)$ is the exterior boundary of the $\mathbb{D}$;
2. $\phi(\gamma_2)$ centers at the origin; and
3. The center of $\phi(\gamma_3)$ is on the imaginary axis.

Definition 4 *(ConformalModule)* The conformal module of the surface S (also the circle domain $\mathbb{D}$) is given by

$$Mod(S) = \{(\mathbf{c_i}, r_i) | i = 1, 2, \ldots, b\}, \tag{5}$$

where $(\mathbf{c_i} = x_i + iy_i, r_i)$ denotes the center and the radius of circle $\phi(\gamma_i)$.

Due to the Möbius normalization, $(\mathbf{c_1}, r_1) = (0 + i0, 1), (\mathbf{c_2}, r_2) = (0 + i0, r_2), (\mathbf{c_3}, r_3) = (0 + iy_3, r_3)$, then the Teichmüller space of genus zero surfaces with b boundaries is of $3b - 6$ dimensional. For a doubly connected domain, the circle domain by conformal mapping is a unit annulus; its conformal module is of 1 dimensional, defined as

$$\frac{-\log r_2}{2\pi}. \tag{6}$$

Theorem 2 (Teichmüller Space Seppala et al. (1992)) *The dimension of the Teichüller space of genus zero surface with b boundaries, $T_{0,b}$, is 1 if $b = 2$, and $3b - 6$ if $b > 2$.*

The Teichmüller space has a so-called Weil-Peterson metric Sharon and Mumford (2006), so it is a Riemannian manifold. Furthermore it is with negative sectional curvature, therefore, the geodesic between arbitrary two points is unique.

2.3 Surface Ricci Flow

Surface Ricci flow is the powerful tool to compute uniformization. *Ricci flow* refers to the process of deforming Riemannian metric $\mathbf{g}$ proportional to the curvature, such that the curvature K evolves according to a heat diffusion process, eventually the curvature becomes constant everywhere. Suppose the metric $\mathbf{g} = (g_{ij})$ in local coordinate. Hamilton (1988) introduced the Ricci flow as

$$\frac{dg_{ij}}{dt} = -K g_{ij}. \tag{7}$$

Surface Ricci flow conformally deforms the Riemannian metric, and converges to constant curvature metric (Chow et al. 2006). Furthermore, Ricci flow can be used to compute the unique conformal Riemannian metric with the prescribed curvature.

Theorem 3 (Hamilton and Chow (Chow et al. 2006)) *Suppose S is a closed surface with a Riemannian metric. If the total area is preserved, the surface Ricci flow will converge to a Riemannian metric of constant Gaussian curvature.*

2.4 Teichmüller Shape Descriptor

Suppose $\Gamma = \{\gamma_0, \gamma_1, \ldots, \gamma_b\}$ is a family of non-intersecting smooth closed curves on a genus zero closed surface. Γ segments the surface to a set of connected components $\{\Omega_0, \Omega_1, \ldots, \Omega_b\}$, each segment Ω_i is a genus zero surface with boundary components. Construct the uniformization mapping $\phi_k : \Omega_k \to \mathbb{D}_k$ to map each segment Ω_k to a circle domain $\mathbb{D}_k$, $0 \le k \le b$. Assume γ_i is the common boundary between Ω_j and Ω_k, then $\phi_j(\gamma_i)$ is a circular boundary on the circle domain $\mathbb{D}_j$, $\phi_k(\gamma_i)$ is another circle on $\mathbb{D}_k$. Let $f_i|_{\mathbb{S}^1} := \phi_j \circ \phi_k^{-1}|_{\mathbb{S}^1} : \mathbb{S}^1 \to \mathbb{S}^1$ be the diffeomorphism from the circle to itself, which is called the *signature of γ_i*. The above construction process is called *conformal welding*.

Journal: 11263 MS: 0586 TYPESET DISK LE CP Disp.:2012/10/24 Pages: 16 Layout: Large

Definition 5 *(Signature of a Family of Loops)* The signature of a family of non-intersecting closed 3D curves $\Gamma = \{\gamma_0, \gamma_1, \ldots, \gamma_b\}$ on a genus zero closed surface is defined as the combination of the conformal modules of all the connected components and the diffeomorphisms of all the curves:

$$S(\Gamma) := \{f_0, f_1, \ldots, f_b\} \cup \{Mod(\mathbb{D}_0), Mod(\mathbb{D}_1), \ldots, Mod(\mathbb{D}_b)\}. \tag{8}$$

The following **main theorem** plays fundamental role for the current work. Note that if a circle domain $\mathbb{D}_k$ is disk, then its conformal module can be omitted from the signature.

Theorem 4 (Main Theorem) *The family of smooth 3D closed curves Γ on a genus zero closed Riemannian surface is determined by its signature $S(\Gamma)$, unique up to a conformal automorphism of the surface $\eta \in Conf(S)$.*

The proof of Theorem 4 can be found in the Appendix section. The main theorem states that the proposed signature determine shapes up to a Möbius transformation. We can further do a normalization that fixes ∞ to ∞ and that the differential carries the real positive axis at ∞ to the real positive axis at ∞, as in Sharon and Mumford's paper (Sharon and Mumford 2006). The signature can then determine the shapes uniquely up to translation and scaling.

The shape signature $S(\Gamma)$ gives us a *complete* representation for the space of shapes. It inherits a natural metric. Given two shapes Γ_1 and Γ_2. Let $S(\Gamma_i) := \{f_0^i, f_1^i, \ldots, f_k^i\} \cup \{Mod(\mathbb{D}_0^i), Mod(\mathbb{D}_1^i), \ldots, Mod(\mathbb{D}_k^i)\}$ $(i = 1, 2)$. We can define a metric $d(S(\Gamma_1), S(\Gamma_2))$ between the two shape signatures using the natural metric in the Teichmüller space, such as the Weil-Petersson metric Sharon and Mumford (2006). Our signature is stable under geometric noise. Our algorithm depends on conformal maps from surfaces to circle domains using discrete Ricci flow method.

3 Algorithm

In this section, we explain the computing details of Teichmüller shape descriptor. Given a genus zero 3D surface with a family of closed curves, the whole domain is first divided by the closed curves into several connected components. We compute the conformal mapping for each connected component by circular uniformization; then after Möbius normalization, compute the conformal modules for each circle domain, and the diffeomorphisms for each closed curve. The pipeline is shown in Fig. 1.

3.1 Circular Uniformization Mapping

We apply discrete Ricci flow method Jin et al. (2008) to conformally map the surfaces onto planar circle domains

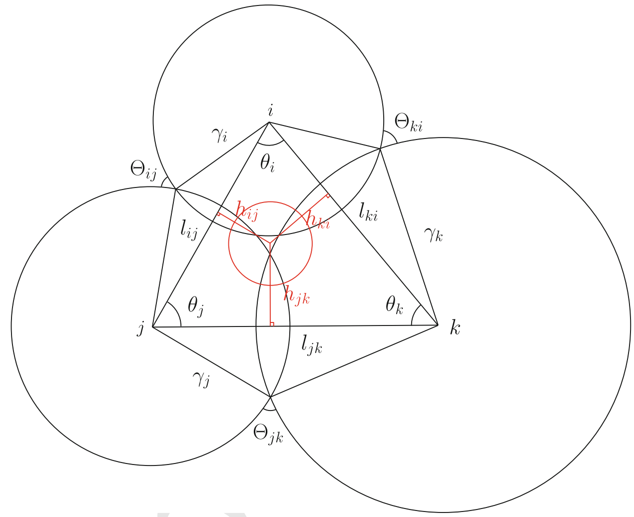

Fig. 2 Discrete Ricci flow with circle packing metric. For the triangle face $[v_i, v_j, v_k]$, each vertex v_i with a circle (v_i, r_i), where r_i is the radius,v_i is the center; on each edge $[v_i, v_j]$, two circles (v_i, r_i) and (v_j, r_j) intersect at an acute angle Θ_{ij}. The red circle is orthogonal to the three circles at three vertices

$\phi_k : S_k \to \mathbb{D}$. The surface is represented as a triangle mesh Σ. A discrete Riemannian metric is represented as the edge length. For each face $[v_i, v_j, v_k]$, the edge lengths satisfy the triangle inequality: $l_{ij} + l_{jk} > l_{ki}$. The angles on each face is determined by the edge lengths according to the cosine law. The discrete Gaussian curvature K_i at a vertex $v_i \in \Sigma$ can be computed as the angle deficit,

$$K_i = \begin{cases} 2\pi - \sum_{[v_i,v_j,v_k]\in\Sigma} \boldsymbol{\theta}_i^{jk}, & v_i \notin \partial\Sigma \\ \pi - \sum_{[v_i,v_j,v_k]\in\Sigma} \boldsymbol{\theta}_i^{jk}, & v_i \in \partial\Sigma \end{cases} \tag{9}$$

where $\boldsymbol{\theta}_i^{jk}$ represents the corner angle attached to vertex v_i in the face $[v_i, v_j, v_k]$, and $\partial\Sigma$ represents the boundary of the mesh. The Gauss–Bonnet theorem (Gu et al. 2004) states that the total curvature is a topological invariant. It still holds on meshes, as follows:

$$\sum_{v_i \in V} K_i = 2\pi\chi(\Sigma), \tag{10}$$

where $\chi(\Sigma)$ denotes the Euler characteristic number of Σ, with $\chi = 2 - 2g - b = 2 - b$ (genus $g = 0$), boundary number $b > 0$.

The discrete Ricci flow can be carried out through circle packing metric, which is a discretization of conformality and was introduced by Thurston (1980). As shown in Fig. 2, we associate each vertex v_i with a circle (v_i, r_i), where r_i is the radius. Let $u_i = \log r_i$ be the discrete conformal factor. Let $[v_i, v_j]$ be an edge, two circles (v_i, r_i) and (v_j, r_j) intersect at an acute angle Θ_{ij}. The edge length is given by

$$l_{ij} = \sqrt{r_i^2 + r_j^2 + 2r_i r_j \cos\Theta_{ij}}. \tag{11}$$

Journal: 11263 MS: 0586 ☐ TYPESET ☐ DISK ☐ LE ☐ CP Disp.:2012/10/24 Pages: 16 Layout: Large

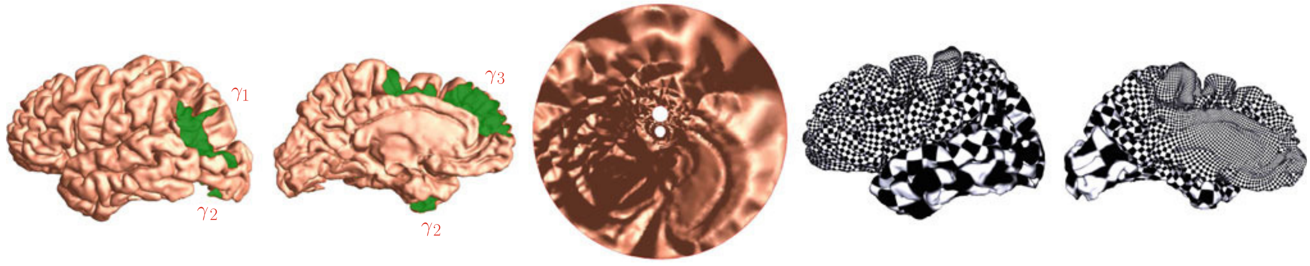

(a) input (front-back view) **(b)** circle domain **(c)** checker-board texture mapping

Fig. 3 Circular uniformization mapping for a brain cortical surface with 3 boundaries. (**a**) shows the front and back views of the input 3D surface which is a genus zero surface with 3 boundaries, $\gamma_i, i = 1, 2, 3$. (**b**) shows the circle domains of conformal mapping results of the input surface, where each 3D boundary is mapped to a circle, γ_1 is mapped to the exterior unit circle, γ_2 and γ_3 are mapped to interior circles. (**c**) shows the front and back views of the checker-board texture mapping results induced by the conformal mapping. The right angles of checker-board are well preserved on the texture mapping results, which demonstrates the angle preserving property of conformal mapping

The discrete Ricci flow is defined as follows:

$$\frac{du_i(t)}{dt} = (\bar{K}_i - K_i), \tag{12}$$

where $\bar{K}_i$ is the user defined target curvature and K_i is the curvature induced by the current metric. The discrete Ricci flow has exactly the same form as the smooth Ricci flow, which conformally deforms the discrete metric according to the Gaussian curvature. The computation is based on circle packing metric Jin et al. (2008).

Suppose Σ is a genus zero mesh with multiple boundary components. The uniformization conformal mapping $\phi : \Sigma \to \mathbb{D}$, where $\mathbb{D}$ is the circle domain, can be computed using Ricci flow by setting the prescribed curvature as follows: (a) The geodesic curvature on the exterior boundary is $+1$ everywhere; (b) the geodesic curvature on other boundaries are negative constants; (c) the Gaussian curvature on interior points are zeros everywhere. Figure 3 shows an example. We use this method to compute conformal mapping, then get conformal module and diffeomorphism descriptor. The main challenge is that the target curvature is dynamically determined by the metric. The metric is evolving, so is the target curvature. The conformal mapping for a genus zero mesh with only one boundary components can be computed similarly. The detailed algorithm is reported in Wang et al. (2012).

3.2 Computing Teichmüller Shape Descriptor

After the computation of the conformal mapping, each connected component is mapped to a circle domain. We compute the Teichmüller shape descriptor as in Eq. 8.

We define an order for all the non-intersecting closed curves on the surface S, $\{\gamma_0, \gamma_1, \gamma_2, \ldots, \gamma_b\}$, this induces an order for all the boundary components on each segment, $\{S_0, S_1, S_2, \ldots, S_b\}$. By removing all the segments from S, the left segment is denoted as $\bar{S}$, which is a multiple connected domain.

For the multiple connected segments (genus zero surfaces with multiple boundaries), the circle domain is the unit disk with multiple inner holes. Two circle domains are conformally equivalent, if and only if they differ by a Möbius transformation. Suppose the boundaries of a circle domain D are $\partial D = \gamma_0 - \gamma_1 - \gamma_2 \ldots - \gamma_b$, each γ_k is a circle $(\mathbf{c}_k, r_k)$, where $\mathbf{c}_k$ denotes the center, r_k denotes the radius. By the definition for the conformal module of a circle domain, we normalize each circle domain using a Möbius transformation, such that γ_0 becomes the unit exterior circle, $\mathbf{c_1}$ is at the origin, $\mathbf{c_2}$ is on the imaginary axis. Then the normalized circle domain is determined by its conformal module (Zeng et al. 2008), which can be computed directly as in Eq. 5,

$$Mod(D) = \{\mathbf{c}_k, k > 1\} \cup \{r_j, j > 0\}. \tag{13}$$

For those simply connected segments (genus zero surfaces with only one boundary), the circle domain is the unit disk. We compute its mass center and use a Möbius transformation to map the center to the origin. Their conformal modules can be omitted in the shape signature.

Each closed curve γ_k on the 3D surface becomes the boundary components on two segments, both boundary components are mapped to a circle under the uniformization mapping. Then each boundary component gives a diffeomorphism of the unit circle to itself, defined as the mapping between the radial angles on two circles,

$$Diff(\gamma_k) = (\theta_k^1, \theta_k^2), \theta_k^1, \theta_k^2 \in [0, 2\pi]. \tag{14}$$

In order to keep consistency, we define a marker p_k on the boundary as the starting point, i.e., $\theta_k^1(p_k) = \theta_k^2(p_k) = 0$, to compute the radial angles for the whole curve.

Journal: **11263** MS: **0586** ☐ TYPESET ☐ DISK ☐ LE ☐ CP Disp.:**2012/10/24** Pages: **16** Layout: **Large**

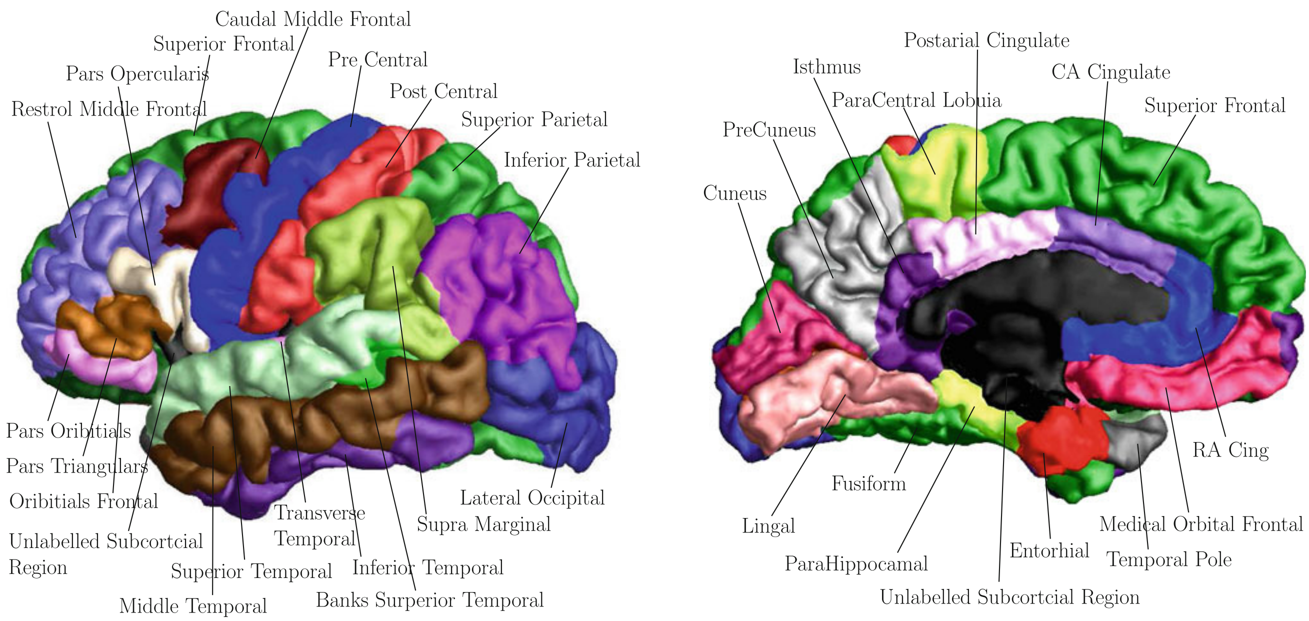

(a) superior view **(b)** inferior view

Fig. 4 Illustration of function areas on the left half brain cortex

4 Experimental Results

We demonstrate the efficiency and efficacy of our method by analyzing the human brain cortical surfaces of AD patients and healthy control subjects. The brain cortical surfaces are represented as triangular meshes. We implement the algorithm using generic C++ on windows XP platform, with Intel Xeon CPU 3.39GHz, 3.98G RAM. The numerical systems are solved using Matlab C++ library. In our experiments, it takes less than one minute to compute the Teichmüller shape descriptor, including the conformal modules and the diffeomorphism curves, for a brain hemisphere surface with 3 contours with $100K$ triangles, as illustrated in Fig. 1. In the following, we explain data source, data processing, experimental setting and results, and performance comparison.

4.1 Data Source

Data used in the preparation of this article were obtained from the ADNI database (http://www.adni.loni.ucla.edu). The ADNI was launched in 2003 by the National Institute on Aging (NIA), the National Institute of Biomedical Imaging and Bioengineering (NIBIB), the Food and Drug Administration (FDA), private pharmaceutical companies and non-profit organizations, as a $60 million, 5-year public-private partnership. The primary goal of ADNI has been to test whether serial MRI, positron emission tomography, other biological markers, and clinical and neuropsychological assessment can be combined to measure the progression of mild cognitive impairment (MCI) and early AD. Determination of sensitive and specific markers of very early AD progression is intended to aid researchers and clinicians to develop new treatments and monitor their effectiveness, as well as lessen the time and cost of clinical trials.

The Principal Investigator of this initiative is Michael W. Weiner, MD, VA Medical Center and University of California at San Francisco. ADNI is the result of efforts of many co-investigators from a broad range of academic institutions and private corporations, and subjects have been recruited from over 50 sites across the U.S. and Canada. The initial goal of ADNI was to recruit 800 adults, ages 55–90, to participate in the research, approximately 200 cognitively normal older individuals to be followed for 3 years, 400 people with MCI to be followed for 3 years and 200 people with early AD to be followed for 2 years. For up-to-date information, see http://www.adni-info.org.

4.2 Data Preprocessing

The structural MRI images were from the ADNI (Jack et al. 2007; Mueller et al. 2005). We tested our algorithm on ADNI baseline image dataset. We used Freesurfer's automated processing pipeline (Fischl et al. 1999; Dale et al. 1999) for automatic skull stripping, tissue classification, surface extraction, and cortical and subcortical parcellations. It also calculates volumes of individual grey matter parcellations in mm^3 and surface area in mm^2, provides surface and volume statistics for about 34 different cortical structures, and computes geometric characteristics such as curvature,

Journal: 11263 MS: 0586 TYPESET DISK LE CP Disp.:2012/10/24 Pages: 16 Layout: Large

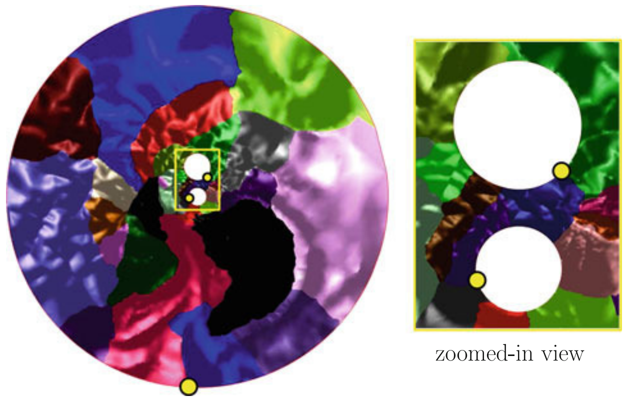

Fig. 5 Markers for computing curve diffeomorphisms. The marker for a curve is selected as a point on the curve which is the intersection of three functional areas. In our test, the markers for the applied three curves are shown as the *yellow points*

curvedness, local foldedness for each of the parcellations (Desikan et al. 2006).

According to the introduction in Desikan et al. (2006), we labeled different cortical surface functional areas in different colors. Figure 4 demonstrates different function area on a left half brain. In this work, we studied the correlations of different regions of brain cortical surface for group difference analysis.

4.3 Experimental Setting

We tested the discrimination ability of the proposed shape descriptor on a set of left brain hemispheres of 152 healthy control subjects and 169 AD patients. Each half brain surface mesh has $100K$ triangles. Among 34 cortical functional areas, we selected 3 regions of interest for study, such as superior frontal, fusiform and inferior parietal areas as shown in Fig. 1, correspondingly, represented by 3 closed curves, $\gamma_1, \gamma_2, \gamma_3$, on the half brain surfaces. In this work, we used the *left* brain hemisphere surfaces for testing shape descriptors.

These three closed curves segment a brain hemisphere surface to 4 patches; one topological annulus (called the base domain), three topological disks. The base domain with three boundaries is mapped to a circle domain, one boundary to the exterior unit circle, one boundary to the inner concentric circle, the rest one to the inner circle centered at the imaginary axis. The conformal module of the base domain is computed as in Eq. 13. In the conformal mapping of each topological disk segment, the mass center is mapped to the origin of the unit disk. In addition, one marker on each curve is extracted as the starting point of computing radial angles. Here, we automatically selected the intersection point of three specified regions along the curve, as shown in Fig. 5. The diffeomorphism descriptor for each curve, computed by Eq. 14, is plotted as a monotonic curve within the square $[0, 2\pi] \times [0, 2\pi]$. We sampled the curve to be $1,000$ points uniformly. Figure 6 illustrates the shape descriptors for 3 healthy control cortical surfaces and 3 AD brain surfaces.

4.4 Numerical Analysis of Signatures among AD and Healthy Control Subjects

We first analyzed the signature itself thoroughly through the data obtained from the AD and healthy control subject groups by considering their distribution and their difference between groups. The statistical difference of signatures between groups are evaluated using t tests.

The proposed signature includes two parts, one is curve diffeomorphism $Diff$, the other is conformal module Mod, i.e., c_i and r_i. Conformal modules describe surface patch separately, while curve diffeomorphisms represent the correlation between surface patches. The c_i and r_i as a whole form the conformal module signature; it is invariant to scaling, rotation, and translation, and is unique up to Möbius transformations. Considering only c_i or r_i will loose much geometric information of each surface patch; when applied for AD classification, neither will get satisfying result, e.g., much less than 63.60 % of (Mod) in Table 2 in our experiment. For the completeness of signature and the coherence to theory, we usually consider c_i and r_i as a whole, the so-called conformal modules, and combine them with the curve diffeomorphisms to form the Teichmüller signature in a local-global view for a 3D surface shape.

In the following we illustrated the discriminative power of signature parameters both separately and compositely by the tests on two subject groups.

As prior AD research reported, the brain atrophy is an important biomarker of AD. Our signature is sensitive to area changes caused by atrophy. Figure 7 gives the box plots of the components of conformal module $Mod = (r_2, y_3, r_3)$, which shows the distribution of each descriptor for each group. The AD group tends to have smaller radii r_i and lower center y_i in the mapping domain; the 95 % confidence intervals for the mean value is given in Table 1. Figure 6 illustrates the curve plots of diffeomorphism signatures. The variations (L2 norm between each pair) among red, green, blue curves reflect the twisting in the gluing process. It is obvious that the variations (twisting) of AD patients' are greater than those of healthy controls. All of these results verify that our new signature is able to capture the brain cortical atrophy related to AD.

To demonstrate the completeness of our new shape signature, we computed the box plots of (Mod), $(Diff)$, and the proposed signature, $(Mod, Diff)$, as shown in 8 for two groups. The shape difference with the complete signature $(Mod, Diff)$ between two groups tends to be more statistically significant with p-value $= 0.0007 < 0.05$ than the signature component (Mod) or $(Diff)$. The results perfectly matched the theoretical expectation.

Journal: **11263** MS: **0586** ☐ TYPESET ☐ DISK ☐ LE ☐ CP Disp.:**2012/10/24** Pages: **16** Layout: **Large**

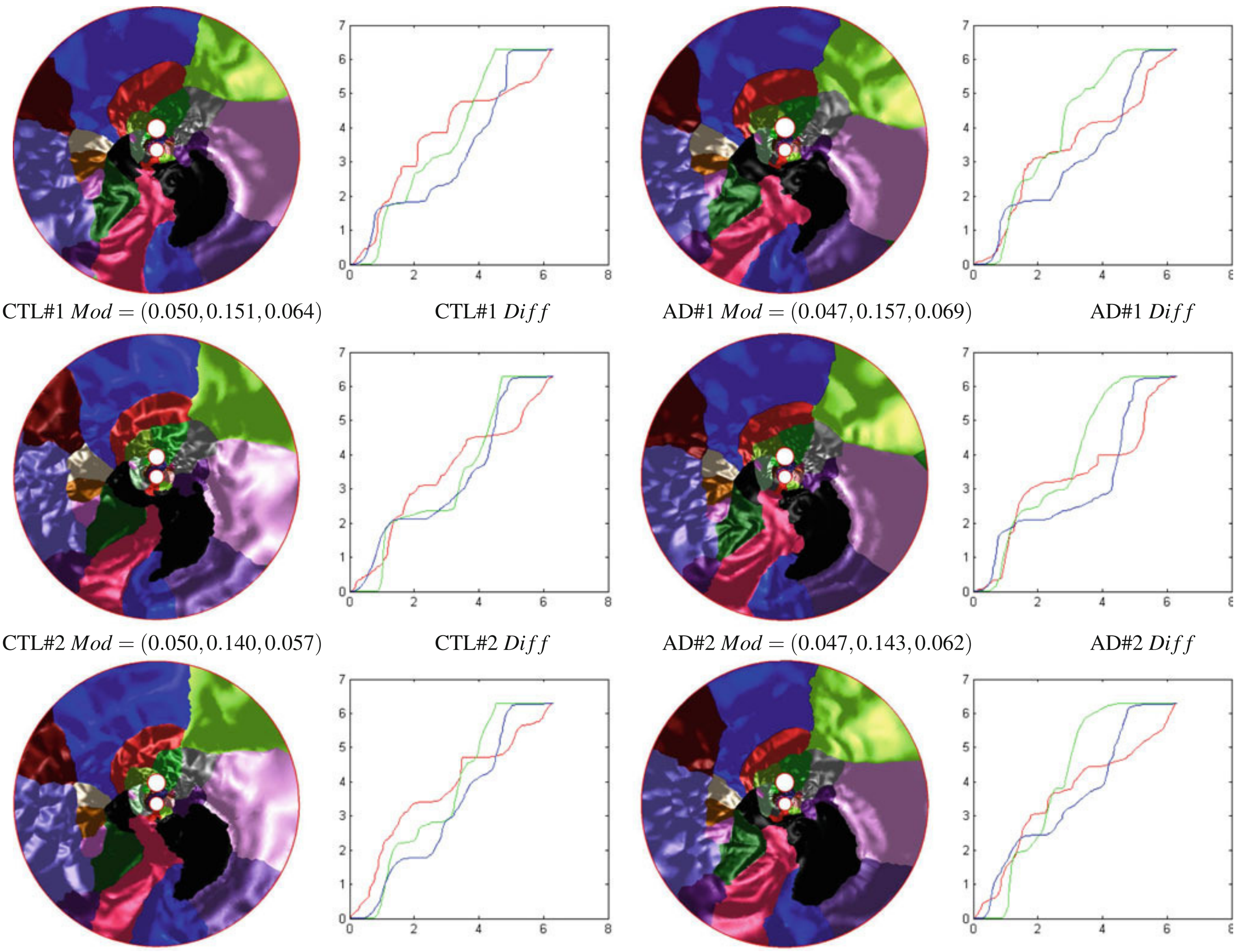

CTL#1 $Mod = (0.050, 0.151, 0.064)$ CTL#1 $Diff$ AD#1 $Mod = (0.047, 0.157, 0.069)$ AD#1 $Diff$

CTL#2 $Mod = (0.050, 0.140, 0.057)$ CTL#2 $Diff$ AD#2 $Mod = (0.047, 0.143, 0.062)$ AD#2 $Diff$

CTL#3 $Mod = (0.049, 0.148, 0.062)$ CTL#3 $Diff$ AD#3 $Mod = (0.046, 0.151, 0.064)$ AD#3 $Diff$

Fig. 6 Teichmüller shape descriptor (Mod, $Diff$) of 3 healthy control (CTL) brain cortexes and 3 Alzheimer's disease (AD) brain cortexes, both of which are randomly selected from the database. The left half brain with 3 contours is considered

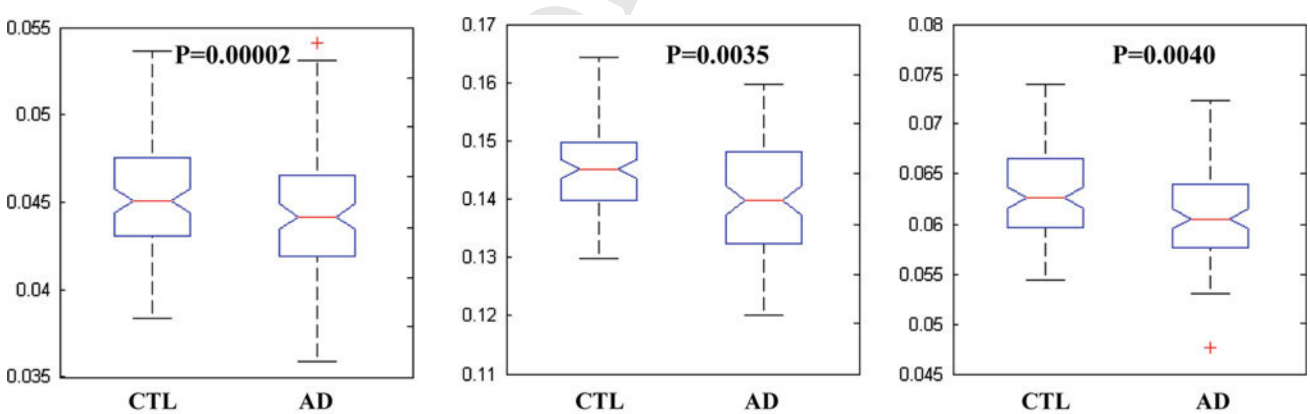

(a) (r_2) **(b)** (y_3) **(c)** (r_3)

Fig. 7 *Box plots* for the distribution of components of conformal module signatures for healthy control subjects and AD patients. (**a**–**c**) describe the *box plots* and p-values for (r_2), (y_3), and (r_3), respectively

Journal: **11263** MS: **0586** TYPESET DISK LE CP Disp.:**2012/10/24** Pages: **16** Layout: **Large**

4.5 Classification among AD and Healthy Control Subjects

For our classification purpose, we set 80 % of each category to be training samples, the rest 20 % testing samples. In order to obtain the fair results, we randomly selected the training set each time and computed the average recognition rate over 1,000 times. We applied the support vector machine (SVM) (http://www.csie.ntu.edu.tw/~cjlin/libsvm/) as classifier, where the linear kernel function was employed, and we used C-SVM and chose $C = 5$ by running cross validation. Table 2 shows that the 95 percent confidence interval for the average recognition rate is 91.38 ± 0.55 %, by the signature $(Mod, Diff)$ under the above experimental setting. We also tested the signatures, diffeomorphism $(Diff)$ and conformal module (Mod), separately. The experimental results demonstrate that the recognition rates are much less than the complete signature $(Mod, Diff)$, which is coherent to the statistical significance analysis as shown in Fig. 8. That satisfies the fact that $(Diff)$ describes the more detailed correlation of each patch to the base domain through the closed curves, while (Mod) captures the global shape information only through the base domain; both together are required to recover the closed curves on 3D surface.

Table 1 The 95 percent confidence intervals for the average values of conformal module components

Sig.	r_2	y_3	r_3
CTL	0.0454 ± 0.0006	0.1477 ± 0.0049	0.0641 ± 0.0022
AD	0.0441 ± 0.0007	0.1404 ± 0.0019	0.0609 ± 0.0009

Table 2 Average recognition accuracy rates (%) for applying different signatures among 152 healthy control subjects versus 169 AD patients, where 80 % of the dataset are randomly selected for training and the rest 20 % for testing

Sig.	$Mod, Diff$	$Diff$	Mod	Vol	$Area$
Rate %	**91.38** ± 0.55	85.71 ± 0.68	63.60 ± 0.60	68.20 ± 0.57	70.23 ± 0.73

The average recognition rate interval with 95 percent confidence is computed over 1,000 times. Linear SVM method is used for classification

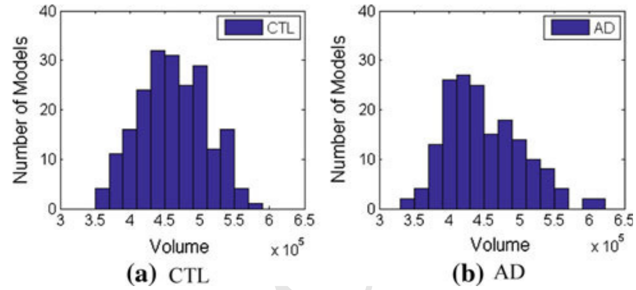

Fig. 9 Histogram of volumes for 152 healthy control (CTL) subjects and 169 Alzheimer's disease (AD) patients

4.5.1 Comparison with Two Simple Brain Measurements

For a simple comparison, we computed the volume for the left brain cortex as a signature, (Vol). The 95 percent confidence interval for the average recognition rate of volume using linear SVM in the above setting is 68.20 ± 0.57 %. The histogram for volume illustrated in Fig. 9 intuitively demonstrates that the volume signature cannot differentiate the AD and healthy control groups accurately. We also computed the surface areas for the base domain and 3 regions as signature $(Area) = (A_0, A_1, A_2, A_3)$; the 95 percent confidence interval for the average recognition rate is 70.23 ± 0.73 %. Although these two statistics are not popular shape descriptors for AD in the literature and a more careful and thorough study such as Cuingnet et al. (2011) and Chincarini et al. (2011) is necessary, the results helped illustrate our

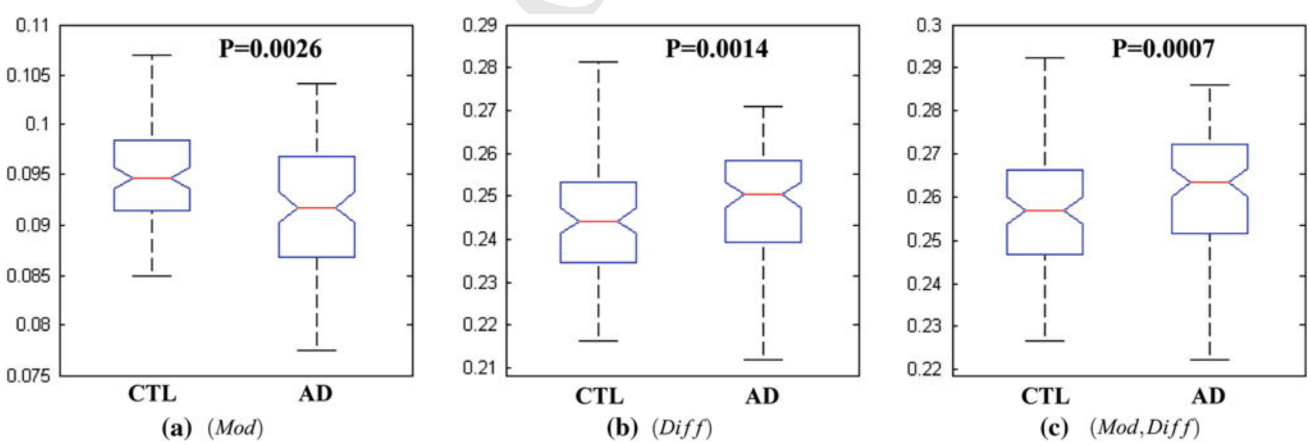

Fig. 8 *Boxplots* for the distribution of components of signatures for healthy control subjects and AD patients. (**a–c**) describe the *box plots* and p-values for signature components (Mod), $(Diff)$, and the complete signature $(Mod, Diff)$, respectively

Journal: **11263** MS: **0586** ☐ TYPESET ☐ DISK ☐ LE ☐ CP Disp.:**2012/10/24** Pages: **16** Layout: **Large**

testing data nature and show the potential of our proposed shape signature.

4.6 Discussion

4.6.1 Stability to Geometric Noise

The proposed work is based on surface Ricci flow research. Computing conformal module is equivalent to solving an elliptic PDE on surfaces. According to geometric elliptic PDE theory, the solution is smoothly depends on the geometry and boundary conditions. In practice, the computation process and the solution are quite stable and robust to geometric noises.

4.6.2 Functional Area Selection

Patients with AD often experience some functional deficits, such as visual deficits, as one of their earliest complaints. Based on this fact, we expect that the AD progress will change the characteristics of some functional areas, and some biomarkers related to AD will emerge. Therefore, we developed the novel and practical tool to verify the correlation between the functional area morphometry and the AD progress.

A full and thorough study of which areas are most related to AD is not the main focus of the current work. We chose the areas mainly based on previous researches. For example, Guo et al. (2010) and Hua et al. (2010) have indicated that the superior temporal area and precuneus and posterior cingulate areas haves significant atrophy in AD group. In Shi et al. (2011), morphometry changes of ten functional areas were studied for their relationship to AD. In our experiments, we selected three areas from the ten areas, fusiform, superior frontal and inferior parietal, and tested our method on these areas. However, our framework is quite general and provides a convenient tool for future research to continue searching other AD-related functional areas.

4.6.3 Biological Meaning of Teichmüller Signature

For surface-based AD research, the state-of-the-art work has used cortical thickness as the measurement Thompson et al. (2003); Cuingnet et al. (2011). However, recent research Winkler et al. (2010) indicated that the commonly used cortical thickness and cortical area measurements are genetically and phenotypically independent. The biological meaning of the proposed shape signature is closely related to brain atrophy so it is more related to cortical area changes.

The proposed signature reflects both local and global geometries and the intrinsic relations among different functional areas. The relation between the signature and the shapes of the areas on cortical surface is highly non-linear and complicated. The atrophy on one functional area will distort the local geometry therefore change the relation to other areas; this relation can be captured by our signature as well. Intuitively, the diffeomorphisms of the circles reflect the gluing pattern among functional areas. The brain atrophy will twist the gluing pattern, and introduces more torsion. For example, in Fig. 6, the variations (twisting) among red, green, blue curves of AD patients' are greater than those of healthy controls. The classification performance with area measurement in Table 2 demonstrates that the AD is related to the functional area changes, which are usually caused by brain atrophy. Therefore, the proposed signature is closely related to brain atrophy.

Our method provides a unique and intrinsic shape signature to study brain morphometry changes caused by brain atrophy. It studies the sensitivity and reproducibility of shape features computed in the entire brain surface domain. The gained insights help improve our understanding to AD related pathology and discover the precise etiology of the grey matter changes. The preliminary results demonstrated that the shape signature provides a reasonably good discriminant power for AD biomarker research.

The method can be equally applied to other regions as well. In future, we may study and compare other functional areas in the medial temporal lobe.

4.6.4 Comparison on AD Detection

Cuingnet et al. (2011) did a thorough study and comparison of 10 methods for AD classification on ADNI; Chincarini et al. (2011) proposed a feature vector which consists of volumes of 9 ROI measurements. Both papers reported impressive results. Although using the same ADNI dataset, a fair and direct comparison between our method and their methods is difficult to perform. Most existing methods focus on the local geometries, whereas our method emphasizes both the local geometries of regions and the relations among them (how to glue them). Our statistical results show that the proposed shape feature is promising as AD shape biomarkers. Whether or not this approach provides more relevant correspondences than those afforded by other measurements (grey matter thickness, ROI such as hippocampal volume) requires careful validation for each application. More importantly, we anticipate that our conformal structure based features may provide new measurements on structural MRI and will be complementary to these other features. We plan to combine them in future for AD classification. If the combined shape features help improve classification accuracy, then it would support the use of conformal structure based measurements such as Teichmüller shape descriptors in AD research.

Journal: 11263 MS: 0586 ☐ TYPESET ☐ DISK ☐ LE ☐ CP Disp.:2012/10/24 Pages: 16 Layout: Large

4.6.5 Future Exploration

For brain cortex morphometry analysis, the current existing methods Cuingnet et al. (2011) mainly rely on grey matter thickness. To the best of our knowledge, this is the first work that features are defined on certain functional area boundaries. From our experience and the earlier work Winkler et al. (2010), our hypothesis is that our new feature would be complementary to thickness measurement. Another interesting question is whether our new shape signature can improve classification on MCI-AD or MCI-healthy control. We plan to continue our exploration further on these two topics in our future work.

5 Conclusions and Future Work

In this paper, we propose a novel method that computes the global shape signatures on specified functional areas on brain cortical surfaces in Teichmüller space. We applied it to study the shape difference of cortical surfaces between AD and healthy control groups. The method is general, robust, and effective; it has great potential to be employed to general brain morphometry study. In the future, we will further explore and validate other applications of this global correlation shape signature in neuroimaging and shape analysis research.

Acknowledgments Data collection and sharing for this project was funded by the Alzheimer's Disease Neuroimaging Initiative (ADNI) (National Institutes of Health Grant U01 AG024904). ADNI is funded by the National Institute on Aging, the National Institute of Biomedical Imaging and Bioengineering, and through generous contributions from the following: Abbott; Alzheimer's Association; Alzheimer's Drug Discovery Foundation; Amorfix Life Sciences Ltd.; AstraZeneca; Bayer Healthcare; BioClinica, Inc.; Biogen Idec Inc.; Bristol-Myers Squibb Company; Eisai Inc.; Elan Pharmaceuticals Inc.; Eli Lilly and Company; F. Hoffmann-La Roche Ltd and its affiliated company Genentech, Inc.; GE Healthcare; Innogenetics, N.V.; Janssen Alzheimer Immunotherapy Research & Development, LLC.; Johnson & Johnson Pharmaceutical Research & Development LLC.; Medpace, Inc.; Merck & Co., Inc.; Meso Scale Diagnostics, LLC.; Novartis Pharmaceuticals Corporation; Pfizer Inc.; Servier; Synarc Inc.; and Takeda Pharmaceutical Company. The Canadian Institutes of Health Research is providing funds to support ADNI clinical sites in Canada. Private sector contributions are facilitated by the Foundation for the National Institutes of Health (http://www.fnih.org). The grantee organization is the Northern California Institute for Research and Education, and the study is coordinated by the AD Cooperative Study at the University of California, San Diego. ADNI data are disseminated by the Laboratory for Neuro Imaging at the University of California, Los Angeles. This research was also supported by NIH grants P30 AG010129, K01 AG030514, and the Dana Foundation. This work has been supported by NSF CCF-0448399, NSF DMS-0528363, NSF DMS-0626223, NSF CCF-0830550, NSF IIS-0916286, NSF CCF-1081424, and ONR N000140910228. Data used in preparation of this article were obtained from the Alzheimer's Disease Neuroimaging Initiative (ADNI) database (adni.loni.ucla.edu). As such, the investigators within the ADNI contributed to the design and implementation of ADNI and/or provided data but did not participate in analysis or writing of this report. A complete listing of ADNI investigators can be found at: http://adni.loni.ucla.edu/wp-content/uploads/how_to_apply/ADNI_Acknowledgement_List.pdf.

6 Appendix: Proof of Theorem 4

Proof See Fig. 10. In the left frame, a family of planar smooth curves $\Gamma = \{\gamma_0, \ldots, \gamma_5\}$ divide the plane to segments $\{\Omega_0, \Omega_1, \ldots, \Omega_6\}$, where Ω_0 contains the ∞ point. We represent the segments and the curves as a tree in the second frame, where each node represents a segment Ω_k, each link represents a curve γ_i. If Ω_j is included by Ω_i, and Ω_i and Ω_j shares a curve γ_k, then the link γ_k in the tree connects Ω_j to Ω_i, denoted as $\gamma_k : \Omega_i \to \Omega_j$. In the third frame, each segment Ω_k is mapped conformally to a circle domain D_k by Φ_k. The signature for each closed curve γ_k is computed $f_{ij} = \Phi_i \circ \Phi_j^{-1}|_{\gamma_k}$, where $\gamma_k : \Omega_i \to \Omega_j$ in the tree. In the last frame, we construct a Riemann sphere by gluing circle domains D_k's using f_{ij}'s in the following way. The gluing process is of bottom up. We first glue the leaf nodes to their fathers. Let $\gamma_k : D_i \to D_j$, D_j be a leaf of the tree. For each point $z = re^{i\theta}$ in D_j, the *extension map* is

$$G_{ij}(re^{i\theta}) = re^{f_{ij}(\theta)}. \tag{15}$$

We denote the image of D_j under G_{ij} as S_j. Then we glue S_j with D_i. By repeating this gluing procedure bottom up, we glue all leafs to their fathers. Then we prune all leaves from the tree, and glue all the leaves of the new tree, and prune again. By repeating this procedure, eventually, we get a tree with only the root node, then we get a Riemann sphere, denoted as S. Each circle domain D_k is mapped to a segment S_k in the last frame, by a sequence of extension maps. Suppose D_k is a circle domain, a path from the root D_0 to D_k is $\{i_0 = 0, i_1, i_2, \ldots, i_n = k\}$, then the map from $G_k : D_k \to S_k$ is given by:

$$G_k = G_{i_0 i_1} \circ G_{i_1 i_2} \circ \ldots \circ G_{i_{n-1} i_n}. \tag{16}$$

Note that, G_0 is identity. Then the Beltrami coefficient of $G_k^{-1} : S_k \to D_k$ can be directly computed, denoted as $\mu_k : S_k \to \mathbb{C}$. The composition $\Phi_k \circ G_k^{-1} : S_k \to \Omega_k$ maps S_k to Ω_k, because Φ_k is conformal, therefore the Beltrami coefficient of $\Phi_k \circ G_k^{-1}$ equals to μ_k.

We want to find a map from the Riemann sphere S to the original Riemann sphere Ω, $\Phi : S \to \Omega$. The Beltrami-coefficient $\mu : S \to \mathbb{C}$ is the union of μ_k's each segments: $\mu(z) = \mu_k(z), \forall z \in S_k$. The solution exists and is unique up to a Möbius transformation according to Quasi-conformal Mapping theorem Gardiner and Lakic (2000). □

Note that, the discrete computational method is more direct without explicitly solving the Beltrami equation. From the Beltrami coefficient μ, one can deform the conformal

Journal: 11263 MS: 0586 ☐ TYPESET ☐ DISK ☐ LE ☐ CP Disp.:2012/10/24 Pages: 16 Layout: Large

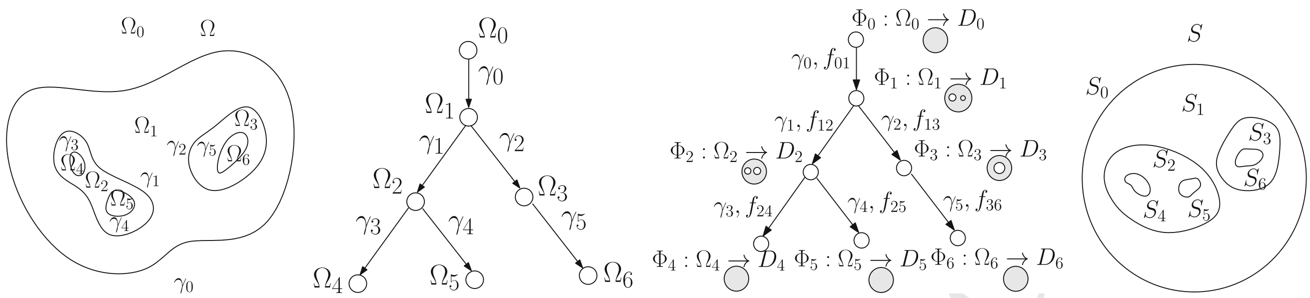

Fig. 10 Proof for the main theorem, the signature uniquely determines the family of closed curves unique up to a Möbius transformation

structure of S_k to that of Ω_k, under the conformal structures of Ω_k, $\Phi : S \to \Omega$ becomes a conformal mapping. The conformal structure of Ω_k is equivalent to that of D_k, therefore, one can use the conformal structure of D_k directly. In discrete case, the conformal structure is represented as the angle structure. Therefore in our algorithm, we copy the angle structures of D_k's to S, and compute the conformal map Φ directly.

References

Angenent, S., Haker, S., Kikinis, R., & Tannenbaum, A. (2000). Nondistorting flattening maps and the 3D visualization of colon CT images. *IEEE Transactions on Medical Imaging, 19*, 665–671.

Ashburner, J., Hutton, C., Frackowiak, R., Johnsrude, I., Price, C., & Friston, K. (1998). Identifying global anatomical differences: Deformation-based morphometry. *Human Brain Mapping*, *6*, 348–357.

Chincarini, A., Bosco, P., Calvini, P., Gemme, G., Esposito, M., Olivieri, C., et al. (2011). Local MRI analysis approach in the diagnosis of early and prodromal Alzheimer's disease. *Neuroimage, 58*(2), 469–480.

Chow, B., Lu, P., & Ni, L. (2006). *Hamilton's Ricci flow*. Providence: American Mathematical Society.

Chung, M. K., Dalton, K. M., & Davidson, R. J. (2008). Tensor-based cortical surface morphometry via weighted spherical harmonic representation. *IEEE Transactions on Medical Imaging, 27*, 1143–1151.

Chung, M. K., Robbins, S. M., Dalton, K. M., Davidson, R. J., Alexander, A. L., & Evans, A. C. (May 2005). Cortical thickness analysis in autism with heat kernel smoothing. *Neuroimage, 25*, 1256–1265.

Cuingnet, R., Gerardin, E., Tessieras, J., Auzias, G., Lehericy, S., Habert, M., et al. (2011). Automatic classification of patients with Alzheimer's disease from structural MRI: A comparison of ten methods using the ADNI database. *Neuroimage, 56*(2), 766–781.

Dale, A. M., Fischl, B., & Sereno, M. I. (1999). Cortical surface-based analysis I: Segmentation and surface reconstruction. *Neuroimage, 27*, 179–194.

Davies, R. H., Twining, C. J., Allen, P. D., Cootes, T. F., & Taylor, C. J. (2003). Shape discrimination in the hippocampus using an MDL model. In *International conference on information processing in medical imaging (IPMI)*. Ambleside.

Desikan, R. S., Segonne, F., Fischl, B., Quinn, B. T., Dickerson, B. C., Blacker, D., et al. (2006). An automated labeling system for subdividing the human cerebral cortex on MRI scans into gyral based regions of interest. *Neuroimage*, *31*, 968–980.

Farkas, H. M., & Kra, I. (1991). *Riemann surfaces (Graduate texts in mathematics)*. New York: Springer.

Fischl, B., Sereno, M. I., & Dale, A. M. (1999). Cortical surface-based analysis II: Inflation, flattening, and a surface-based coordinate system. *NeuroImage, 9*, 195–207.

Fox, N., Scahill, R., Crum, W., & Rossor, M. (1999). Correlation between rates of brain atrophy and cognitive decline in AD. *Neurology*, *52*(8), 1687–1689.

Frisoni, G., Fox, N., Jack, C., Scheltens, P., & Thompson, P. (2010). The clinical use of structural MRI in Alzheimer disease. *Nature Reviews Neurology, 6*(2), 67–77.

Gardiner, F. P., & Lakic, N. (2000). *Quasiconformal Teichmüller theory*. Providence: American Mathematical Society.

Gerig, G., Styner, M., Jones, D., Weinberger, D., & Lieberman, J. (2001). Shape analysis of brain ventricles using SPHARM. In *Proceedings of MMBIA 2001* (pp. 171–178). doi:10.1109/MMBIA.2001.991731.

Gorczowski, K., Styner, M., Jeong, J.-Y., Marron, J. S., Piven, J., Hazlett, H. C., Pizer, S. M., & Gerig, G. (2007). Statistical shape analysis of multi-object complexes. *IEEE computer society conference on computer vision and pattern recognition, CVPR '07* (pp. 1–8). Minneapolis.

Gu, X., Wang, Y., Chan, T. F., Thompson, P. M., & Yau, S.-T. (2004). Genus zero surface conformal mapping and its application to brain surface mapping. *IEEE Transactions on Medical Imaging, 23*, 949–958.

Guo, X., Wang, Z., Li, K., Li, Z., Qi, Z., Jin, Z., et al. (2010). Voxel-based assessment of gray and white matter volumes in Alzheimer's disease. *Neuroscience Letters*, *468*, 146–150.

Hamilton, R. S. (1988). The Ricci flow on surfaces. *Mathematics and General Relativity*, *71*, 237–262.

Henrici, P. (1988). Applied and computational complex analysis (Vol. 3). New York: Wiley-Intersecience.

Hua, X., Lee, S., Hibar, D. P., Yanovsky, I., Leow, A. D., Toga, A. W., et al. (2010). Mapping Alzheimer's disease progression in 1309 MRI scans: Power estimates for different inter-scan intervals. *Neuroimage,51*, 63–75.

Hurdal, M. K., & Stephenson, K. (2004). Cortical cartography using the discrete conformal approach of circle packings. *NeuroImage, 23*, S119–S128.

Jack, C. R. J., Bernstein, M. A., Fox, N. C., Thompson, P. M., Alexander, P. M., Harvey, D., et al. (2007). The Alzheimer's disease neuroimaging initiative (ADNI): MRI methods. *Journal of Magnetic Resonance Imaging, 27*, 685–691.

Jack, C. R, Jr, Shiung, M. M., Gunter, J. L., O'Brien, P. C., Weigand, S. D., Knopman, D. S., et al. (2004). Comparison of different MRI brain atrophy rate measures with clinical disease progression in AD. *Neurology*, *62*, 591–600.

Jin, M., Kim, J., Luo, F., & Gu, X. (September 2008). Discrete surface Ricci flow. *IEEE Transactions on Visualization and Computer Graphics*, *14*, 1030–1043.

Lai, R., Shi, Y., Scheibel, K., Fears, S., Woods, R., Toga, A., & Chan, T. (2010). Metric-induced optimal embedding for intrinsic 3d shape

Journal: 11263 MS: 0586 TYPESET DISK LE CP Disp.:2012/10/24 Pages: 16 Layout: Large

analysis. In *2010 IEEE conference on computer vision and pattern recognition (CVPR)* (pp. 2871–2878). San Francisco.

Liu, X., Shi, Y., Dinov, I., & Mio, W. (2010). A computational model of multidimensional shape. *International Journal of Computer Vision*, *89*, 69–83.

Lui, L. M., Zeng, W., Yau, S.-T. & Gu, X. (2010). Shape analysis of planar objects with arbitrary topologies using conformal geometry. In *11th European conference on computer vision (ECCV 2010)*. Heraklion.

Mueller, S. G., Weiner, M. W., Thal, L. J., Petersen, R. C., Jack, C., Jagust, W., et al. (2005). The Alzheimer's disease neuroimaging initiative. *Neuroimaging Clinics of North America*, *15*, 869–877.

Pizer, S., Fritsch, D., Yushkevich, P., Johnson, V., & Chaney, E. (1999). Segmentation, registration, and measurement of shape variation via image object shape. *IEEE Transactions on Medical Imaging, 18*, 851–865.

Qiu, A., & Miller, M. I. (2008). Multi-structure network shape analysis via normal surface momentum maps. *NeuroImage, 42*, 1430–1438.

Schoen, R., & Yau, S.-T. (1994). *Lectures on differential geometry*. Boston: International Press of Boston.

Schwartz, E. L., Shaw, A., & Wolfson, E. (1989). A numerical solution to the generalized Mapmaker's problem: Flattening nonconvex polyhedral surfaces. *IEEE Transactions on Pattern Analysis and Machine Intelligence, 11*, 1005–1008.

Seppala, M., & T.S. (1992). *Geometry of Riemann surfaces and Teichmüller spaces. North-Holland mathematics studies*. Amsterdam: North-Holland.

Sharon, E., & Mumford, D. (October 2006). 2D-shape analysis using conformal mapping. *International Journal of Computer Vision, 70*, 55–75.

Shen, L., Saykin, A. J., Chung, M. K., & Huang, H. (2007). Morphometric analysis of hippocampal shape in mild cognitive impairment: An imaging genetics study. In *IEEE 7th international conference bioinformatics and bioengineering*. Boston.

Shi, Y., Lai, R., & Toga, A. (2011). Corporate: cortical reconstruction by pruning outliers with reeb analysis and topology-preserving evolution. *Information Process Medical Imaging, 22*, 233–244.

Thompson, P. M. (1996). A surface-based technique for warping 3-dimensional images of the brain. *IEEE Transactions on Medical Imaging*, *15*, 1–16.

Thompson, P. M., Hayashi, K. M., Zubicaray, G. D., Janke, A. L., Rose, S. E., Semple, J., et al. (2003). Dynamics of gray matter loss in Alzheimer's disease. *Journal of Neuroscience*, *23*, 994–1005.

Thurston, W. P. (1980). *Geometry and topology of three-manifolds*. Princeton: Princeton university.

Timsari, B. (2000). Optimization method for creating semi-isometric flat maps of the cerebral cortex. In *SPIE symposium on medical imaging 2000: image processing* (Vol. 3979, pp. 698–708). San Diego.

Tosun, D., Reiss, A., Lee, A. D., Dutton, R. A., Hayashi, K. M., Bellugi, U., et al. (2006). Use of 3-D cortical morphometry for mapping increased cortical gyrification and complexity in Williams syndrome. In *3rd IEEE international symposium on biomedical imaging: From nano to macro 2006* (pp. 1172–1175). Arlington.

Trouve, A., & Younes, L. (2005). Metamorphoses through Lie group action. *Foundations of Computational Mathematics*, *5*, 173–198.

Wang, Y., Gu, X., Chan, T. F., & Thompson, P. M. (2009). Shape analysis with conformal invariants for multiply connected domains and its application to analyzing brain morphology. *IEEE computer society conference on computer vision and pattern recognition, CVPR '09* (pp. 202–209). Miami.

Wang, Y., Gu, X., Chan, T. F., Thompson, P. M., & Yau, S.-T. (2006). Brain surface conformal parameterization with algebraic functions. *Proceedings of medical image computing and computer-assisted intervention Part II* (pp. 946–954). Copenhagen.

Wang, Y., Gu, X., Chan, T. F., Thompson, P. M., & Yau, S.-T. (2008). Conformal slit mapping and its applications to brain surface parameterization. In *Proceedings of international conference on medical image computing and computer-assisted intervention: Part I* (pp. 585–593). New York.

Wang, Y., Lui, L., Gu, X., Hayashi, K. M., Chan, T. F., Toga, A. W., et al. (2007). Brain surface conformal parameterization using Riemann surface structure. *IEEE Transactions on Medical Imaging, 26*, 853–865.

Wang, Y., Shi, J. Yin, X., Gu, X., Chan, T. F., Yau, S.-T., Toga, A. W. & Thompson, P. M. (2012). Brain surface conformal parameterization with the Ricci flow. *IEEE Transcations on Medical Imaging, 31*, 251–264.

Wang, Y., Song, Y., Rajagopalan, P., An, K. L. T., Chou, Y., Gutman, B., et al. (2011). Surface-based tbm boosts power to detect disease effects on the brain: An n=804 ADNI study. *Neuroimage, 56*(4), 1993–2010.

Winkler, A. M., Kochunov, P., Blangero, J., Almasy, L., Zilles, K., Fox, P. T., et al. (2010). Cortical thickness or grey matter volume? The importance of selecting the phenotype for imaging genetics studies. *NeuroImage, 53*(3), 1135–1146.

Zeng, W., Lui, L. M., Gu, X., & Yau, S.-T. (2008). Shape analysis by conformal modules. *International Journal of Methods and Applications of Analysis (MAA),15*(4), 539–556.

Zeng, W., Samaras, D., & Gu, X. D. (2010). Ricci flow for 3d shape analysis. *The IEEE Transactions on Pattern Analysis and Machine Intelligence,32*(4), 662–677.

Journal: **11263** MS: **0586** ☐ TYPESET ☐ DISK ☐ LE ☐ CP Disp.:**2012/10/24** Pages: **16** Layout: **Large**